J. Fluid Mech. (1986), *vol.* 169, *pp.* 323–336
Printed in Great Britain

Dissipative waves in fluids having both positive and negative nonlinearity

By M. S. CRAMER,
Department of Engineering Science and Mechanics, Virginia Polytechnic Institute and State University, Blacksburg, VA 24061, USA

A. KLUWICK,
Institut für Strömungslehre und Wärmeübertragung, Technical University of Vienna, Wiedner Hauptstr. 7, A-1040 Vienna, Austria

L. T. WATSON AND W. PELZ†
Department of Computer Science, Virginia Polytechnic Institute and State University, Blacksburg, VA 24061, USA

(Received 17 July 1985)

We examine weakly dissipative, weakly nonlinear waves in which the fundamental derivative $\bar{\Gamma}$ changes sign. The undisturbed state is taken to be at rest, uniform and in the vicinity of the $\bar{\Gamma} = 0$ locus. The cubic Burgers equation governing these waves is solved numerically; the resultant solutions are compared and contrasted to those of the inviscid theory. Further results include the presentation of a natural scaling law and inviscid solutions not reported elsewhere.

1. Introduction

In recent years, the existence of negative nonlinearity has been predicted for a number of single-phase fluids of practical interest. Negative nonlinearity occurs when the thermodynamic parameter

$$\bar{\Gamma} \equiv \bar{\Gamma}(\bar{\rho}, \bar{s}) \equiv \frac{1}{\bar{\rho}} \frac{\partial(\bar{\rho}\bar{a})}{\partial \bar{\rho}}\bigg|_{\bar{s}}, \tag{1.1}$$

is negative for a range of pressures and temperatures. Here $\bar{\rho}$, $\bar{s}$ and $\bar{a}$ are the dimensional density, entropy and sound speed respectively. The quantity $\bar{\Gamma}$ is frequently referred to as the fundamental derivative of gasdynamics. When $\bar{\Gamma}$ is negative at every point in a body of fluid, wavefronts steepen backwards and expansion or rarefaction shocks are the only discontinuities capable of propagating in the fluid. Two of the earliest studies concerned with such fluids are due to Bethe (1942) and Zel'dovich (1946), who showed that Van der Waals gases exhibit negative nonlinearity provided the specific heats take on sufficiently large values.

Lambrakis & Thompson (1972) and Thompson & Lambrakis (1973) have carried out detailed computations with more accurate equations of state to provide specific examples of gases in which negative nonlinearity may be observed. These were seen to be hydrocarbons and fluorocarbons of moderate complexity. Although more accurate computations may be desirable, the region of interest for single-phase fluids

† Present address: Department of Mathematical Sciences, University of Akron, Akron, OH 44325, USA.

was clearly consistent with the predictions of the previous studies. Recent experimental studies by Borisov *et al.* (1983) have clearly demonstrated the existence of negative nonlinearity in an ostensibly single-phase fluid. In these shock-tube studies, stable expansion shocks were observed in the relatively simple compound Freon-13 ($CClF_3$). However, in this case, the negative nonlinearity is due to the well-known anomalous behaviour of the specific heat and sound speed at the critical point.

Because the fundamental derivative (1.1) is a thermodynamic function, it generally varies from point to point in a disturbance. When the wave amplitudes are sufficiently large, the local value of $\bar{\Gamma}$ can change sign within a single wave or pulse. When this is the case, previous investigations show that the wave dynamics can be surprisingly different from that characteristic of ideal gases. In particular, Thompson & Lambrakis (1973) have predicted the existence of shocks of moderate strength having both upstream and downstream Mach numbers equal to unity. In the following we refer to the condition where the convected sound speed at a shock is identical to the speed of the shock as sonic. Thus, the shocks of Thompson & Lambrakis can be referred to as double sonic shocks. Cramer & Kluwick (1984; hereinafter referred to as I), have developed a complete weak-shock theory for fluids having regions of both positive and negative nonlinearity. This study illustrated the formation and propagation of expansion and compression shocks in the same pulse. Ultimately, the compression and expansion shocks were seen to collide resulting in a single merged shock. The nature of the merged shock depended on the undisturbed state of the fluid. Although the double sonic shocks of Thompson & Lambrakis (1973) are not ordinarily possible for weak waves, shocks having sonic conditions on only one side are in fact possible. The structure of these sonic shocks was determined and it was shown that, on the sonic side, these approach the inviscid conditions algebraically rather than exponentially. Thus, not only are the sonic shocks a new and interesting phenomenon in the inviscid theory, but the viscous structure of these waves contrasts sharply with that of non-sonic shocks. Associated with these sonic shocks are the partial disintegration of both compression and expansion shocks and a complicated dependence on initial conditions which are taken into account by the precursor waves described in I.

When viscosity and heat conduction were considered, it was shown in I that the nonlinear evolution could be described by the cubic Burgers equation discussed in §2. As proved by Nimmo & Crighton (1982), no linearizing Bäcklund transformations can exist which would yield analytical solutions to this equation. Although limited success may be obtained through use of a pure finite difference scheme, the expected difficulties at steep wavefronts cannot be overcome during the most interesting phase of the evolution, namely the collision between compression and expansion shocks. The present paper, therefore, reports the development of a mixed scheme capable of solving this equation under a wide variety of conditions. As an example we apply this to the square wave initial conditions discussed in I and compare the results to the inviscid theory. In doing so we provide an independent verification of the complicated wave evolution predicted by I. Furthermore, we illuminate the viscous structure of the collision between compression and expansion shocks; in the inviscid theory this collision occurs at a single point in space–time.

A complete qualitative and partial quantitative description of the inviscid evolution of a square wave was given in I. In order to give a quantitative comparison of the viscous and inviscid theories, a complete analytical description of the inviscid theory has been obtained and is summarized in §3. Although some of the quantitative results presented may be obtained from I, most are new results not reported

elsewhere. We have also found that a more natural scaling may be found; this is described in §2.

We expect the results presented in I and here to be of interest in other areas of mechanics and engineering. References to related phenomena in solid mechanics, plasma physics and superfluid hydrodynamics have been given in I. In addition to these studies, Kluwick (1986) has derived the analog of (2.2) for the case of long waves in suspensions of solid particles in fluids. Turner (1979, 1981, 1983) has derived an equivalent set of equations for second-sound waves near the b-nodal line in liquid helium. The existence of both compression and expansion shocks for square wave initial conditions was predicted and observed (see also the review by Liepmann & Laguna 1984). An analysis of the shock structure was also given (Turner 1979). A summary of rarefaction shocks in vapour–liquid mixtures has been provided by Thompson, Carofano & Kim (1986).

2. Problem statement

We consider small disturbances in a weakly dissipative Navier–Stokes fluid. The undisturbed state is taken to be uniform and at rest and sufficiently near the $\bar{\Gamma} = 0$ locus. In particular, we take

$$\left.\begin{aligned} \Gamma &\equiv \frac{\rho_0}{a_0}\bar{\Gamma}(\rho_0, s_0) = O\left(\frac{\bar{\rho}-\rho_0}{\rho_0}\right), \\ R &\equiv \frac{\rho_0 a_0 L}{\mu_0} = O\left(\left(\frac{\rho_0}{\bar{\rho}-\rho_0}\right)^{\frac{1}{2}}\right), \end{aligned}\right\} \tag{2.1}$$

where s_0, ρ_0, a_0, μ_0 are the entropy, density, sound speed and shear viscosity evaluated at the undisturbed state. The non-dimensional quantity R is recognized as a wave Reynolds number based on the disturbance length L. In I, it was shown that, under these conditions, the evolution of one-dimensional waves is governed by

$$u_t + (\hat{\Gamma} + \tfrac{1}{2}\Lambda u)\, uu_X = \tfrac{1}{2}\delta u_{XX}, \tag{2.2}$$

where

$$u \equiv \frac{\bar{\rho}-\rho_0}{\epsilon\rho_0}, \quad X \equiv \frac{\bar{x}-a_0\bar{t}}{L}, \quad t \equiv \frac{a_0\epsilon^2\bar{t}}{L}. \tag{2.3}$$

The quantities $\bar{x}$ and $\bar{t}$ are the dimensional position and time and ϵ is a small parameter measuring the disturbance amplitude. The nonlinearity and dissipation constants $\hat{\Gamma}$, Λ and δ are defined as

$$\hat{\Gamma} \equiv \frac{1}{\epsilon}\Gamma, \quad \Lambda \equiv \frac{\rho_0^2}{a_0}\frac{\partial\bar{\Gamma}}{\partial\bar{\rho}}\bigg|_{\bar{s}}(\rho_0, s_0) \quad \text{and} \quad \delta \equiv \frac{1}{R\epsilon^2}\left(\frac{\lambda_0}{\mu_0} + 2 + \frac{\gamma_0 - 1}{Pr}\right), \tag{2.4}$$

where γ_0, λ_0, Pr are the values of the ratio of specific heats, second viscosity and Prandtl number evaluated at the undisturbed state. A comparison of (2.4) with (2.1) shows that $\hat{\Gamma}$, Λ and δ are all of order one in the limit of small ϵ. Here we recognize $\hat{\Gamma}$ and δ as scaled versions of the fundamental derivative and acoustic diffusivity, respectively.

A typical initial condition for this problem is given by

$$\frac{\bar{\rho}-\rho_0}{\rho_0} = \epsilon A F\left(\frac{\bar{x}}{L}\right),$$

where F is a non-dimensional function of its argument and A is a second non-dimensional amplitude parameter taken to be of order one. It should be recognized

that such a separation of the wave amplitude into separate amplitude parameters is somewhat artificial. However, it will be convenient to use ϵ to fix the overall amplitude levels; the second parameter will then be chosen to fix the specific wave amplitude. The function F may be taken to have a maximum absolute value of 1. When the non-dimensionalizations (2.3) are applied, the initial condition becomes

$$u(X,0) = AF(X). \tag{2.5}$$

Equations (2.2) and (2.5) form the initial-value problem governing the evolution of weak waves in which $\bar{\Gamma}$ takes on both positive and negative values. In order to simplify the discussion, a set of rescalings were proposed in I. The resulting dependent and independent variables were termed universal variables. When these rescalings are applied to (2.2) and (2.5) it is found that the solution depends on three non-dimensional groups. Since then a more convenient and informative set of rescalings has been discovered. If we define new variables

$$v = \frac{A}{\hat{\Gamma}}u, \quad \xi = \frac{1}{\sigma}X, \quad \tau = \frac{\hat{\Gamma}^2}{|A|}\bar{t}, \tag{2.6}$$

(2.2) and (2.5) become

$$\left.\begin{aligned} v_\tau + (1+\tfrac{1}{2}v)vv_\xi &= \tfrac{1}{2}\delta_e v_{\xi\xi}, \\ v(\xi,0) &= A_e F(\sigma\xi), \end{aligned}\right\} \tag{2.7}$$

where σ denotes the sign of A, i.e. $A/|A|$, and

$$\left.\begin{aligned} \delta_e = \delta\frac{|A|}{\hat{\Gamma}^2} &= \frac{|A|}{R\Gamma^2}\left(\frac{\lambda_0}{\mu_0}+2+\frac{\gamma_0-1}{Pr}\right), \\ A_e &= \frac{AA\epsilon}{\Gamma}. \end{aligned}\right\} \tag{2.8}$$

In terms of the physical variables, the density disturbance will be given by

$$\frac{\bar{\rho}-\rho_0}{\rho_0} = \frac{\Gamma}{A}\mathscr{F}\left(\frac{\bar{x}-a_0\bar{t}}{\sigma L}, \frac{\Gamma^2 a_0}{L|A|}\bar{t}; A_e, \delta_e, \sigma\right), \tag{2.9}$$

where the function $\mathscr{F}$ is given by the solution to (2.7). Thus, solutions corresponding to the same function F will be self-similar provided both the amplitude and dissipation similarity parameters (2.8) are the same. It is also a formal requirement that the sign of A, i.e. σ, must be the same for the two flows, although this is not likely to be a major constraint. Typical initial conditions of interest are symmetric about $\bar{x} = 0$. In this case, $F(\sigma\xi)$ in (2.7) may be replaced by $F(\xi)$ and the functional form of the final solution will not depend on σ. The advantage of this rescaling over the universal variables used in I is that the number of similarity parameters is reduced, provided we disregard σ, from three to two. Furthermore, because the scaling on X is essentially independent of the nonlinearity parameters, the dissipation parameter δ_e is a true measure of the actual dissipation; this again contrasts with the variables presented in I. A final advantage is that $\delta_e L$ and $A_e/A\epsilon$ are determined completely by the thermodynamic state of the undisturbed fluid. Thus, the similarity parameters (2.8) may be varied independently by varying only the length and amplitude of the initial waveform.

In this paper, we examine the special case of a square wave having a total length equal to L. The function F will therefore be taken to be

$$F(p) = \begin{cases} 1 & -\frac{1}{2} \leqslant p \leqslant \frac{1}{2}, \\ 0 & \text{otherwise.} \end{cases} \tag{2.10}$$

In order to focus on the main nonlinear effects we will take the undisturbed state and the length of the wave to be fixed. In terms of the similarity parameters, this means that δ_e and σ will be fixed. In the examples discussed, the value of the small parameter will also be fixed; and the wave amplitude, and therefore A_e, will be varied by choosing various values of A.

3. Inviscid solutions

In I it was shown that inviscid motions of these fluids are governed by the characteristic relation

$$v = \text{constant on } \frac{\mathrm{d}\xi}{\mathrm{d}\tau} = v + \tfrac{1}{2}v^2, \tag{3.1}$$

the expression for the shock speed

$$\frac{\mathrm{d}\xi_s}{\mathrm{d}\tau} = \tfrac{1}{2}(v_a + v_b) + \tfrac{1}{6}(v_a^2 + v_a v_b + v_b^2), \tag{3.2}$$

and the speed ordering relation

$$\left.\frac{\mathrm{d}\xi}{\mathrm{d}\tau}\right|_a > \frac{\mathrm{d}\xi_s}{\mathrm{d}\tau} \geqslant \left.\frac{\mathrm{d}\xi}{\mathrm{d}\tau}\right|_b. \tag{3.3}$$

Equations (3.1)–(3.3) have been cast in terms of the similarity variables given in (2.6). The subscripts a and b denote conditions after and before the shock respectively. As in I, the designations a and b must be interchanged when $\sigma < 0$; this is due to the reflection of the $\bar{x}$-axis in (2.6). The function $\xi_s = \xi_s(\tau)$ represents the shock trajectory in (ξ, τ)-space. Results (3.1) and (3.2) were derived in I through an analysis of the exact inviscid equations. The speed ordering relation (3.3) is used to rule out inadmissible discontinuities. In terms of the inviscid theory, this was taken to be a highly plausible postulate. However, it was also shown in I that (3.3) emerges naturally from the analysis of the viscous structure of these shocks, i.e. it is a necessary condition for the existence of a viscous structure of the discontinuities.

The equality in (3.3) is the condition for sonic shocks. By combining (3.1)–(3.3), the strength and speed of sonic shocks can be shown to be

$$[v] = \tfrac{3}{2}(v_a + 1), \tag{3.4}$$

$$\frac{\mathrm{d}\xi_s}{\mathrm{d}\tau} = \left.\frac{\mathrm{d}\xi}{\mathrm{d}\tau}\right|_b = \tfrac{1}{8}(v_a + 3)(v_a - 1), \tag{3.5}$$

where the brackets will denote jumps in the indicated quantity, i.e. $[Q] \equiv Q_a - Q_b$. These are an explicit expression of the fact that the strength and speed of sonic shocks are determined uniquely by the conditions on only one side of the shock.

When applied to the square-wave initial condition (2.10), the inviscid equations (3.1)–(3.3) yield four qualitatively different cases. When $A_e > -1$, the local value of $\bar{\Gamma}$ has the same sign everywhere in the pulse. As one would expect, the final waveform is either a compression or expansion shock, which interacts with, and is eroded by,

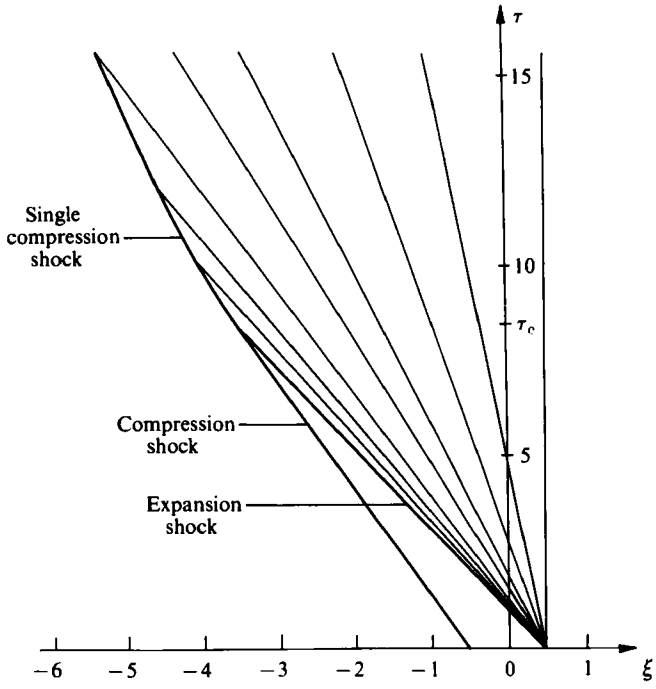

FIGURE 1. Typical (ξ, τ)-diagram for case (i) $-\frac{3}{2} < A_e < -1$. Unless indicated otherwise, all solid lined are characteristics defined by (3.1).

a centred expansion or compression fan. In order to focus on the new phenomena predicted in I, we will confine our attention to the remaining amplitude ranges listed below

$$\left.\begin{aligned} &\text{(i)} \quad -\tfrac{3}{2} \leqslant A_e \leqslant -1, \\ &\text{(ii)} \quad -3 \leqslant A_e \leqslant -\tfrac{3}{2}, \\ &\text{(iii)} \quad A_e \leqslant -3. \end{aligned}\right\} \tag{3.6}$$

The corresponding (ξ, τ)-diagrams are given in figures 1–3. It should be noted that these are merely representative sketches to illustrate the general behaviour in each amplitude range and should not be used for quantitative purposes. Computed density distributions are provided in figures 4–6. These are plotted in terms of the original variables (2.3) and are typical of undisturbed states having $\hat{\Gamma} > 0$, $\Lambda < 0$.

For these values of $\hat{\Gamma}$, Λ, the density distribution of case (i) consists of a compression shock, a constant density region and an expansion shock followed by a centred expansion fan; see, for example, figures 1 and 4. The strength of the expansion shock is given by (3.4) with $v_a = A_e$. In terms of the similarity variables, the time at which these shocks collide is $24(A_e+3)^{-2}$. After this time the shock interacts with the centred fan. To compute this interaction, we set $v_a = 0$ in (3.2) and recognize that v_b is given by the centred fan. A second expression for the shock speed is derived by evaluating the integrated form of the characteristic relations (3.1) at the shock. When these expressions for the shock speed are equated, we find that the density perturbation before the shock, $v_b = v(\xi_s(\tau), \tau) \equiv G(\tau)$, satisfies

$$\frac{\mathrm{d}G}{\mathrm{d}\tau} = -\frac{G}{6\tau}\frac{3+2G}{1+G}.$$

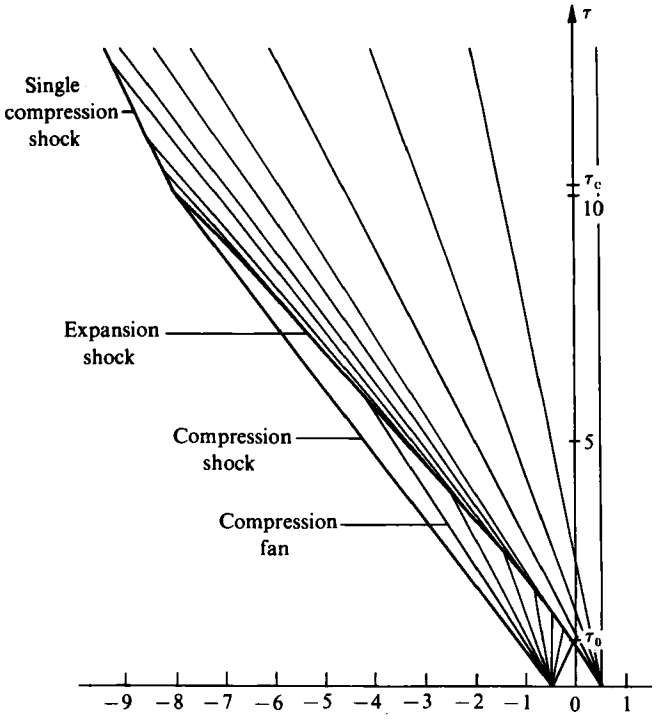

FIGURE 2. Typical (ξ, τ)-diagram for case (ii) $-3 < A_e < -\frac{3}{2}$. Unless indicated otherwise, all solid lines are characteristics defined by (3.1).

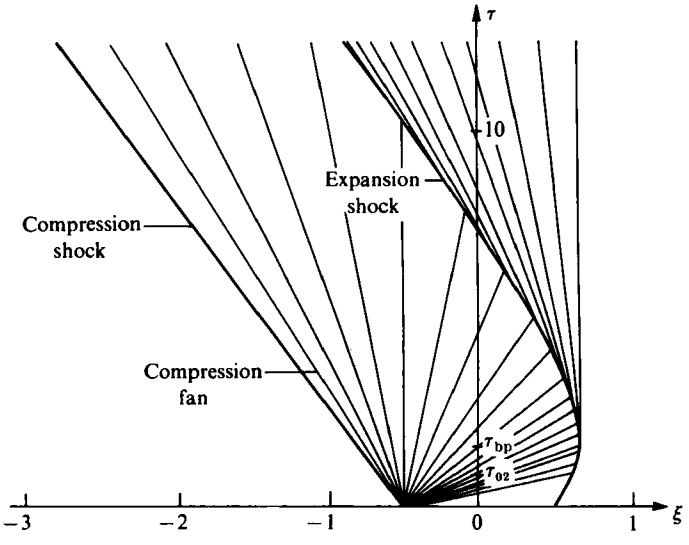

FIGURE 3. Typical (ξ, τ)-diagram for case (iii) $A_e < -3$. Unless indicated otherwise, all solid lines are characteristics defined by (3.1).

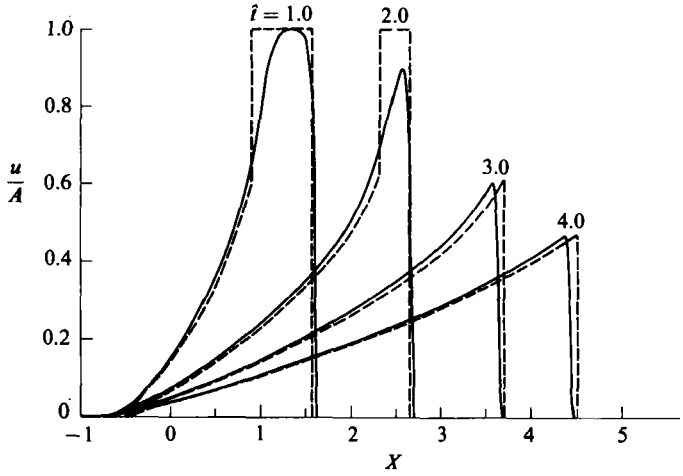

FIGURE 4. Square wave evolution for $A = 0.77$, $A_e = -1.32$. Collision time is $\hat{t} \approx 2.94$. Dotted lines denote inviscid solution. Solid lines denote computed viscous solution.

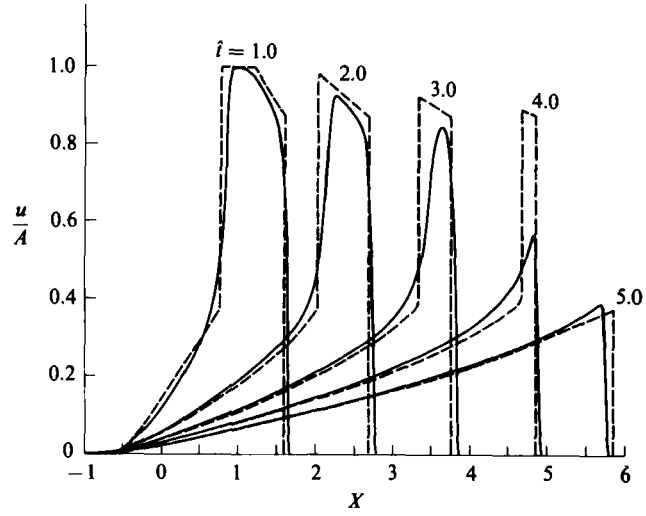

FIGURE 5. Square wave evolution for $A = 1.0$, $A_e = -1.72$. Collision time is $\hat{t} \approx 4.68$. Precursor is present from $\hat{t} \approx 1.77$ to $\hat{t} \approx 5.04$. Dotted lines denote inviscid solution. Solid lines denote computed viscous solution.

Immediately after collision (see figures 1 and 4), v_b is given by the first wave of the centred fan. Thus the initial condition for the interaction is

$$v_b = G = -\tfrac{1}{2}A_e + 3 \quad \text{at } \tau = \frac{24}{(A_e+e)^2}.$$

When the above differential equation for G is integrated and the initial condition is employed, the decay law for the fan–shock interaction is found to be

$$\tau G^2(G+\tfrac{3}{2}) = -3A_e. \tag{3.7}$$

An analogous version of (3.7) was derived in I for the case $A_e > 0$. It can be shown that the general form of (3.7), i.e. that obtained by replacing the right-hand side by

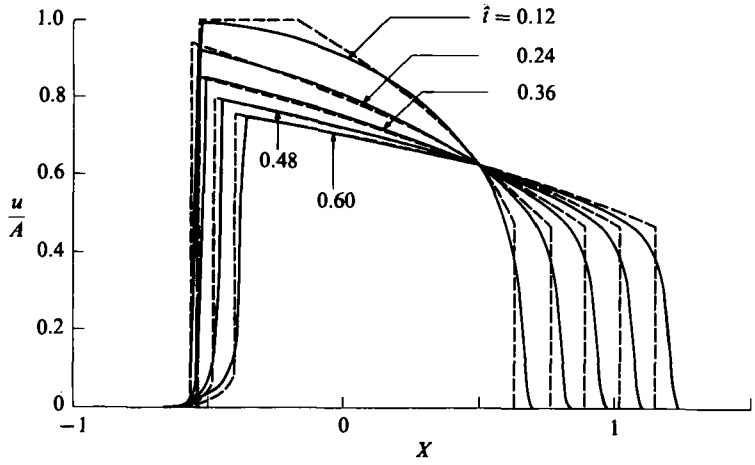

FIGURE 6. Square wave evolution for $A = 1.86$, $A_e = -3.20$. Expansion shock becomes stationary at $\hat{t} \approx 0.24$. Collision time is $\hat{t} \approx 9.86$. Dotted lines denote inviscid solution. Solid lines denote computed viscous solution.

a general integration constant, holds for all interactions between centred fans and non-sonic shocks. That is, the general result is independent of the particular point of origin of the fan, the nature of the shock and fan, i.e. whether compression or expansion, or the details leading to the interaction.

In case (ii), the waveform consists of a sonic compression shock, followed by a centred compression fan, followed by a constant density region. The return to the undisturbed state is accomplished through a sonic expansion shock and centred expansion fan; see figures 2 and 5. The expansion shock first penetrates the compression fan at time

$$\tau_0 = \frac{8}{3}\frac{1}{(1+A_e)^2}, \tag{3.8}$$

which yields a decay rate which appeared as equation (4.8) in I. In similarity variables this reads

$$[v] = \tfrac{3}{2}(1+A_e)\left(\frac{\tau_0}{\tau}\right)^{\frac{3}{8}}; \tag{3.9}$$

the expressions for v_a, v_b may be obtained by combining (3.9) with (3.4). The derivation of (3.9) is essentially the same as that for (3.7). The main difference is that (3.5) must be employed in place of (3.2). As in the case of (3.7), the general form of the decay law (3.9), i.e.

$$[v] = \text{constant} \times \tau^{-\frac{3}{8}},$$

holds for all possible interactions between sonic shocks and centred fans.

For $\tau > \tau_0$, the sonic expansion shock is followed by a non-centred expansion referred to as a precursor which, in turn, is followed by the centred expansion fan. The term precursor is due to the fact that this wave always occurs before the expansion shock in either the universal variables of I or the similarity variables introduced here; see, e.g. figure 2. The flow in the precursor region is determined by integrating (3.1) to yield the usual parametric description of the density distribution; the parameter employed in this study was the time at which a sound wave represented by the characteristic line is emitted from the expansion shock.

The sonic expansion shock collides with the sonic compression shock at time

$$\tau_c = \tau_0(-2(1+A_e))^{\frac{3}{3}}, \tag{3.10}$$

where τ_0 is given by (3.8). For $\tau_{ep} > \tau > \tau_c$ the merged shock interacts with the precursor which had previously separated the expansion shock from the expansion fan. Here τ_{ep} is the time at which the last wave of the precursor intersects the merged shock and is given by

$$\tau_{ep} = \frac{24}{(A_e+3)^2}; \tag{3.11}$$

this turns out to be identical to the collision time for case (i). The interaction between the precursor and merged shock is governed by

$$\tau G^2(G+1)^{\frac{2}{3}} = 9\times 4^{-\frac{8}{3}}\tau_c, \tag{3.12}$$

where $v_a = 0, v_b = G(\tau)$ and τ_c is given by (3.10). The derivation of the decay law (3.12) is similar to that of (3.7). The main difference is that the centred fan must be replaced by the precursor wave. For $\tau > \tau_{ep}$, the merged shock interacts with the centred expansion fan. The resultant decay law turns out to be identical to (3.7). It should be noted that results (3.11) and (3.12) were not explicitly given in I.

In the course of the above derivations, it was found that the slope of the density distribution in the precursor is always infinite at the expansion shock. In fact, we have shown that

$$\frac{\partial v}{\partial \xi} \sim \frac{1}{4}\left(\frac{3}{\tau}\right)^{\frac{1}{2}} \frac{1}{(\xi-\xi_{es}(\tau))^{\frac{1}{2}}} + \ldots,$$

as $\xi \to \xi_{es}$, where $\xi_{es}(\tau)$ is the position of the sonic expansion shock at scaled time τ. This vertical slope may be observed in figure 5 at the times $t = 3.0$, 4.0. It is also present at time $t = 2.0$, but the width of the precursor region is only $\Delta X \approx 2\times 10^{-3}$ and is not noticeable on the scale of the figure. At $t = 1.0$, the expansion shock is still non-sonic and the precursor has not yet appeared.

A second set of results not reported in I are the details of the solution for case (iii). Because of the nonlinear dependence of the shock speed on its strength, the expansion shock is initially non-sonic and propagates at a speed smaller than the sound speed of the undisturbed media. As a result, it moves to the left relative to the wave coordinates employed in figures 3 and 6. The compression shock is sonic and is followed by a centred compression fan. At a scaled time,

$$\tau_{02} = \frac{3}{A_e(A_e+\frac{3}{2})}, \tag{3.13}$$

the expansion shock intersects the compression fan. This shock weakens according to a decay law similar to (3.7) and, at time

$$\tau_{bp} = -\tfrac{2}{9}A_e, \tag{3.14}$$

the expansion shock stops, becomes sonic, and begins moving to the right in figure 6. For $\tau_{bp} < \tau < \tau_{c2}$, the density distribution is given by a sonic compression shock followed by a centred compression fan, followed by the sonic expansion shock and precursor. The decay law for the expansion shock is similar to (3.9) and the strength of the compression shock remains constant. Here τ_{c2} is the scaled time at which the expansion and compression shock collide and is given by

$$\tau_{c2} = -\tfrac{2^{19}}{9^3}A_e. \tag{3.15}$$

For $\tau > \tau_{c2}$, the flow is governed by the interaction of the merged shock with the precursor emitted by the expansion shock at previous times. The decay law for this shock is essentially the same as (3.12) with a different integration constant; this reads

$$\tau G^2(1+G)^{\frac{2}{3}} = -2A_e, \tag{3.16}$$

where $v_a = 0$, $v_b = G(\tau)$. We note that results (3.13)–(3.16) are new in the sense that they were not given explicitly in I.

In closing, we note that in each of cases (i)–(iii) the final decay is given by

$$v \sim \left(-\frac{2A_e}{\tau}\right)^{\frac{1}{2}}$$

as $\tau \to \infty$. This is easily verified by an inspection of the decay laws (3.7) and (3.16). Thus, in spite of the qualitatively different transient behaviour, the final evolution is always the same.

4. Numerical scheme

The governing equation, (2.2) or (2.7), is parabolic; thus both stability and accuracy must be considered when selecting a numerical algorithm. Reasonable alternatives include finite difference, Galerkin, collocation and spectral methods. A mixed-type algorithm using spline collocation in space and finite differences in time was chosen. Splines were chosen as the approximating basis functions because they provide high-order approximation power, are efficiently evaluated and are adaptable in the sense that their approximation power can be localized in small intervals; see, e.g. deBoor (1978). The presence of moving shocks makes this latter characteristic particularly attractive.

For fixed time $\hat{t}$, $u(X,\hat{t})$ was approximated as follows

$$u(X,\hat{t}) \approx \sum_{i=1}^{n} \alpha_i B_i(X),$$

where B_i, $i = 1,\ldots,n$, are cubic B-spline basis functions defined on a knot sequence, $\chi_1, \chi_2, \ldots, \chi_{n+4}$, that extends well beyond the shock on both sides and 'adapts' to follow the shock. Both the number $n+4$ and the position of the knots varies with time and the severity of the shock; the knot spacing is very small in the vicinity of the shock. For a specified accuracy of 10^{-4}, a typical value of n was 500. Adaptive cubic spline collocation is a very sophisticated algorithm; complete details may be found in Ascher (1980) and Ascher, Christiansen & Russell (1981*a*, *b*).

For stability, $u_{\hat{t}}$ was approximated by the backward difference,

$$\frac{u(X,\hat{t}) - u(X,\hat{t}-\Delta\hat{t})}{\Delta\hat{t}},$$

which results in the implicit equation

$$u_{XX}(X,\hat{t}) = \frac{2}{\delta}\left\{\frac{u(X,\hat{t}) - u(X,\hat{t}-\Delta\hat{t})}{\Delta\hat{t}} + (1+\tfrac{1}{2}u(X,\hat{t}))\,u(X,\hat{t})\,u_X(X,\hat{t})\right\}, \tag{4.1}$$

with boundary conditions $u(X,\hat{t}) \to 0$ as $X \to \pm\infty$. The quantity $u(X,\hat{t}-\Delta\hat{t})$ will be known from the previous timestep. The overall scheme is to replace $u_{\hat{t}}$ by a backward difference, replace $u(X,\hat{t})$ by a spline, enforce the boundary conditions and enforce the implicit nonlinear equation (4.1) at an appropriate number of discrete points. The

resulting nonlinear algebraic system of equations is then solved by a quasi-Newton algorithm (see, e.g. Moré, Garbow & Hillstrom 1980; Dennis & Schnabel 1983; Watson, Kamat & Reaser 1986). The error in this computed approximation to $u(X, \hat{t})$ is then estimated. If the estimated error exceeds a specified tolerance, the number of knots is increased and the knot distribution is modified to improve the approximation; details of this are found in Ascher *et al.* (1981*b*). Finally, the entire process is repeated until the error satisfies the imposed tolerance levels.

The mathematical software employed was the adaptive spline collocation package COLSYS; see, e.g. Ascher *et al.* (1981*b*). This was accurate and robust for the present problem, although was occasionally found to be inefficient. The number of collocation points was seen to vary between 100 and 1000.

5. Results

Sample calculations of square wave initial conditions (2.10) are depicted in figures 4–6; the variables appearing there are those defined in (2.3). For purposes of illustration, we have set the parameters (2.4) to be

$$\hat{\Gamma} = 5.0, \quad A = -8.6, \quad \delta = 5 \times 10^{-3}.$$

In terms of the similarity variables appearing in (2.8), we find $\sigma = -1$, $\delta_e = 1.72 \times 10^{-3}$. The effective dissipation will therefore be the same for each case discussed. The differences observed in each case will be primarily due to nonlinear effects.

The inviscid and viscous solutions for the case $A = 0.77$ are plotted in figure 4. Because $A_e \approx -1.32$, this corresponds to case (i) in §3. The values of $\hat{t}$ have been specifically chosen to illustrate the viscous structure of the collision between the sonic expansion shock and the leading compression shock. At $\hat{t} = 1.0$, the merging process is already in its initial stages. For this case, the inviscid theory, discussed in §3, predicts a collision time of 2.94. It was found that the merging process was essentially complete by this time. After the collision time the inviscid and viscous solutions are in reasonable agreement. More detailed computations show that this is also the case for times sufficiently less than that at which the viscous collision begins. Here we note that the expansion shock is somewhat thicker than the compression shock. This is due, in part, to the fact that the strength of the former is less than half of the latter. The second factor is the fact that the expansion shock is sonic. It was shown in I that sonic and near-sonic conditions lead to inherently thicker shocks.

In the second example, we have taken $A = 1$ which implies $A_e = -1.72$. The evolution of this case is depicted in figure 2. Equations (3.8) and (3.10) may be combined with the scalings (2.6) to verify that the collision time is $\hat{t} \approx 4.68$. Again, the numerical calculations show that the viscous collision is essentially complete by this time. At subsequent times, the viscous and inviscid solutions were again seen to agree well.

The last example has amplitudes $A = 1.86$, $A_e \approx -3.2$ and is plotted in figure 6. Here we have chosen the times to illustrate the retrograde motion of the expansion shock. If we combine the scalings (2.6) with (3.13) and (3.14), we find that the expansion shock penetrates the compression fan at a time $\hat{t} \approx 0.19$, at which time it begins to weaken and slow. At $\hat{t} \approx 0.24$ its stops and begins to propagate to the right. Thus, the profile at $\hat{t} = 0.24$ is that slightly before the expansion shock becomes stationary. At times $\hat{t} = 0.36$–0.60, the smooth part of the expansion is carried out through the precursor, although this is readily seen only at the later two time

intervals. Here the infinite slope at the expansion shock may also be observed. At $v = -2$, $u/A \approx 0.625$, the inviscid solution is known to be stationary in the wave coordinates employed here. It is interesting to note that the computed viscous solutions are also stationary there. This appears to be analogous to the result that the inviscid nodes of a periodic wave are frequently those of the viscous solution as well.

6. Conclusions

The results of this paper fall into three categories. The first is the presentation of a more convenient set of scalings for the viscous theory; see (2.6)–(2.8). The effects of nonlinearity and dissipation are characterized by the similarity parameters A_e and δ_e. Once the thermodynamic state of the undisturbed fluid is specified, the first is determined by specifying the wave amplitude and the second by the length of the wave. We expect these similarity relations will be useful in relating results obtained in experimental and numerical studies.

The second set of new results are the analytic solutions of the inviscid equations (3.1)–(3.3). These may be viewed as a continuation and completion of the analytic work carried out in I.

The analytic solutions of the inviscid equations play an essential role in the realization of the final and main goal of this paper, namely the computation of dissipative solutions to (2.2) and the comparison of these solutions to the inviscid theory. The numerical scheme described in §4 has been found to be a powerful tool in the study of dissipative waves in fluids having both positive and negative nonlinearity. This conclusion is based on the success reported here as well as its application to the simpler case of step function initial conditions and the more complicated case of shock formation and propagation. Because the mesh adapts to the solution as it is generated, the scheme is seen to be capable of describing multiple, non-stationary shocks without the difficulties encountered in simpler, e.g. finite-difference, schemes. The results presented provide a description of the viscous collision between expansion and compression shocks; it was found that this is typically complete by the collision time predicted by the inviscid theory. Except for the time during which this collision takes place the solutions are seen to be in close agreement. Thus, a third important contribution is that this provides an independent verification of the predictions of the inviscid theory given in I.

REFERENCES

Ascher, U. 1980 Solving boundary value problems with a spline-collocation code. *J. Comp. Phys.* **34**, 401.

Ascher, U., Christiansen, J. & Russell, R. D. 1981*a* Collocation software for boundary-value ODEs. *ACM Trans. Math. Software* **7**, 209–222.

Ascher, U., Christiansen, J. & Russell, R. D. 1981*b* Algorithm 569. COLSYS: Collocation software for boundary-value ODEs. *ACM Trans. Math. Software* **7**, 223.

Bethe, H. A. 1942 The theory of shock waves for an arbitrary equation of state. *Office Sci. Res. and Dev. Rep.* 545.

Borisov, A. A., Borisov, Al. A., Kutateladze, S. S. & Nakoryakov, V. E. 1983 Rarefaction shock wave near the critical liquid–vapour point. *J. Fluid Mech.* **126**, 59–73.

Cramer, M. S. & Kluwick, A. 1984 On the propagation of waves exhibiting both positive and negative nonlinearity. *J. Fluid Mech.* **142**, 9–37.

deBoor, C. 1978 *A Practical Guide to Splines.* Springer.

DENNIS, J. E. & SCHNABEL, R. 1983 *Numerical Methods for Unconstrained Optimization and Nonlinear Equations.* Prentice-Hall.

KLUWICK, A. 1986 Weakly nonlinear kinematic waves in suspensions of particles in fluids. *Phys. Fluids* (submitted).

LAMBRAKIS, K. C. & THOMPSON, P. A. 1972 Existence of real fluids with a negative fundamental derivative Γ. *Phys. Fluids* **5**, 933–935.

LIEPMANN, H. W. & LAGUNA, G. A. 1984 Nonlinear interactions in the fluid mechanics of Helium II. *Ann. Rev. Fluid Mech.* **16**, 139–177.

MORÉ, J. J., GARBOW, G. S. & HILLSTROM, K. E. 1980 *User Guide for MINPACK-1 ANL-80-74.* Argonne National Laboratory.

NIMMO, J. J. C. & CRIGHTON, D. G. 1982 Bäcklund transformations for nonlinear parabolic equations: the general results. *Proc. R. Soc. Lond.* A **384**, 381–401.

THOMPSON, P. A., CAROFANO, G. C. & KIM, Y.-G. 1986 Shock waves and phase changes in a large-heat-capacity fluid emerging from a tube. *J. Fluid Mech.* **166**, 57–92.

THOMPSON, P. A. & LAMBRAKIS, K. C. 1973 Negative shock waves. *J. Fluid Mech.* **60**, 187–208.

TURNER, T. N. 1979 Second-sound shock waves and critical velocities in liquid Helium II. Ph.D. dissertation, California Institute of Technology, Pasadena.

TURNER, T. N. 1981 New experimental results obtained with second-sound shock waves. *Physica* **107** B, 701–702.

TURNER, T. N. 1983 Using second-sound shock waves to probe the intrinsic critical velocity of liquid Helium II. *Phys. Fluids* **26**, 32.27–32.41.

WATSON, L. T., KAMAT, M. P. & REASER, M. H. 1986 A robust hybrid algorithm for computing multiple equilibrium solutions. *Engng Comput.* (to appear).

ZEL'DOVICH, YA. B. 1946 On the possibility of rarefaction shock waves. *Zh. Eksp. Teor. Fiz.* **4**, 363–364.